Shear stress in arterial stenoses: a momentum integral model

ELSEVIER

Journal of Biomechanics 31 (1998) 1051–1057

JOURNAL OF BIOMECHANICS

Shear stress in arterial stenoses: a momentum integral model

Jason M. Reese*, David S. Thompson

Department of Engineering, University of Aberdeen, Fraser Noble Building, Aberdeen AB24 3UE, U.K.

Received in final form 17 April 1998

Abstract

A mathematical model is developed to investigate blood flow in arterial stenoses up to Reynolds numbers of 1000. The approach is based on Thwaites' method, normally used to treat laminar boundary layer development over a body in a freestream. The model is applicable to any axisymmetric stenosis geometry in all laminar physiological flow regimes, has a minimum of externally input parameters and is implemented as a short program on a personal computer. Maximum bounds on the expected errors are derived by comparison with known results from Poiseuille flow in a pipe. Agreement with shear stresses reported by other researchers using computational fluid dynamics is within 13% rms. The method has been specifically designed to be a useful predictive tool for biomedical investigators.

Keywords: Wall shear stress; Stenoses; Momentum integral method; Blood flow; Mathematical model

1. Introduction

Atherosclerotic disease is characterised by localised arterial narrowing. The flow of blood through these stenoses has been the subject of much research, because increased fluid shear stresses near the stenosis 'neck' or 'throat' can activate blood platelets and induce thrombosis (Ku, 1997). The behaviour of human endothelial cells may also be shear-stress dependent (Houston et al., 1999). Values of shear stress are needed so that clinical pathological evidence can be matched to laboratory experiments.

As wall shear stresses are difficult to measure, and then only accurate to within 20–50% (Ku, 1997), researchers have relied on computational fluid dynamics (CFD) and analytical models to estimate shear stress throughout the stenosis (Back and Crawford, 1992; Damodaran et al., 1996; Huang et al., 1995; Johnston and Kilpatrick, 1991). CFD models numerically solve the fundamental equations of blood flow through a stenosis and are therefore presumed to produce the most accurate predictions of shear stress. However, these simulations can be time-consuming and impractical when used systematically to explore shear stress dependence on area reduction, stenosis length, mean flow velocity and so on. Conversely, analytical models derived from laminar boundary layer theory produce predictions which do not always agree with CFD for all physiological flow conditions. There remains a clear need for a straightforward and accurate predictive model of blood flow through stenoses, using a minimum of adjustable parameters.

We propose a new mathematical model for the calculation of shear stresses in stenoses which can be easily implemented on a personal computer or a programmable calculator by biomedical researchers, but which still captures the physics of the blood flow.

2. Mathematical model

2.1. Modelling assumptions

For a medium-sized artery the Reynolds number typically varies from 100 to 1000 (Ku, 1997) so blood flow in human circulation is not normally turbulent (Skalak et al., 1989). We shall therefore assume that the flow throughout the stenosis is laminar, and that laminar boundary layer equations apply.

We also assume that the artery is stiff and can be modelled as a rigid cylindrical tube with smooth walls (Ku, 1997). Real stenoses have an irregular profile but

* Corresponding author.

0021-9290/98/$ – see front matter
PII: S0021-9290(98)00130-4

a smooth and rigid axisymmetric stenosis is a common approximation (Johnston and Kilpatrick, 1991). We also assume that the flow through the artery and stenosis is steady, although the real flow is pulsatile. In any case, maximum shear stress in the stenosis is expected to occur when the arterial flow is at maximum flow rate. Blood flow achieves a fully developed Poiseuille velocity profile some distance from the origin of the artery at either a valve or branch. Therefore, the flow which enters the stenosis can be assumed to have developed from a fluid stagnation point some distance upstream.

The changing character of the wall flow in the short stenosis region is particularly suited to boundary layer treatment as the strong acceleration of the mean flow markedly thins the viscous region. The velocity profile changes from the parabolic Poiseuille form to a flatter profile typical of flows with an inviscid core. This changing velocity profile has been confirmed by theoretical studies (Morgan and Young, 1974) and numerical and experimental simulations (Huang et al., 1995; Johnston and Kilpatrick, 1991).

Finally, for the high shear encountered in a stenosis, blood acts as an incompressible Newtonian fluid of constant viscosity. It is only at low shear that blood displays non-Newtonian behaviour and increased viscosity (Rosenson et al., 1996).

A diagram of the stenosed artery is shown in Fig. 1. Poiseuille flow is achieved by point 1. some distance downstream of a stagnation point 0 but just upstream of a stenosis. The axially symmetric, smooth, conical stenosis represents a constant monotonic area contraction from point 1 to point 2. Blood accelerates and the pressure falls from inlet to throat, where the velocity reaches its maximum and the pressure gradient drops to zero. Beyond the stenosis the flow slows down again and there may be boundary layer separation.

2.2. The momentum integral equation

The boundary layer equations represent conservation of mass and momentum in the layer of blood retarded by the artery wall. In the cylindrical coordinate system (z, y) of Fig. 1, assuming negligible circumferential variations of fluid quantities, the equations of motion of steady flow of an incompressible Newtonian fluid are (White, 1991)

$$\frac{1}{y}\frac{\partial}{\partial y}(yu_y) + \frac{\partial u_z}{\partial z} = 0, \tag{1}$$

$$u_y\frac{\partial u_z}{\partial y} + u_z\frac{\partial u_z}{\partial z} = -\frac{1}{\rho}\frac{dp}{dz} + \frac{\mu}{\rho}\left(\frac{1}{y}\frac{\partial}{\partial y}\left(y\frac{\partial u_z}{\partial y}\right) + \frac{\partial^2 u_z}{\partial z^2}\right), \tag{2}$$

where u_y and u_z are the inward radial and axial components of fluid velocity, p is the hydrostatic pressure, ρ is the density of blood and μ is its (constant) dynamic viscosity.

In the region of Poiseuille flow (point 1 in Fig. 1), the effects of viscosity penetrate the entire width of the artery whereas in the stenosis a flattened velocity profile reflects a boundary layer that is thin in comparison with the artery width (Fig. 2). We assume that in both cases the centreline (axial) velocity is the 'freestream' outside the boundary layer and is governed by Bernoulli's equation

$$\frac{dp}{dz} = -\rho U\frac{dU}{dz}, \tag{3}$$

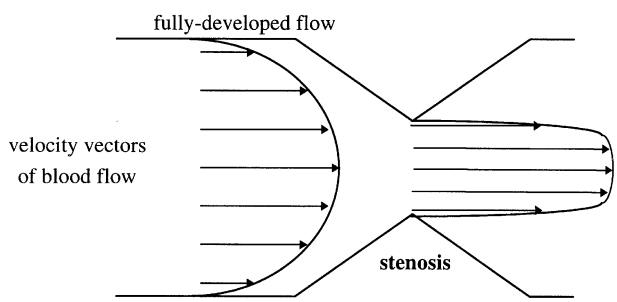

Fig. 2. Schematic diagram of velocity profiles in the artery and stenosis. Upstream of the stenosis is Poiseuille flow, with a parabolic profile. The flow profile at the throat has a flatter core, with high shear at the wall.

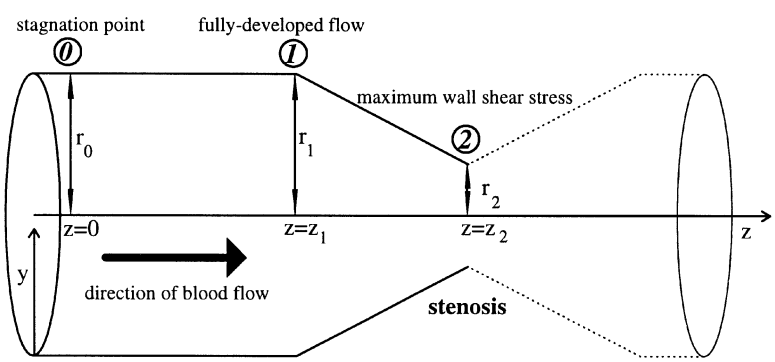

Fig. 1. Schematic diagram of the artery and stenosis cross-section. The system is cylindrical, with y inwardly radial and z axial.

where $U = U(z)$ is the centreline velocity. We ignore the small drop in stagnation pressure over the short contraction.

With the usual boundary layer assumptions we neglect the $\partial^2 u_z/\partial z^2$ term in comparison to the $\partial^2 u_z/\partial y^2$ term in Eq. (2). Substituting Eq. (3) into Eq. (2), then multiplying Eq. (1) by $(U - u_z)$, subtracting the result from Eq. (2), and integrating the resulting equation from $y = 0$ at the artery wall to e.g. $y = r_0$, the radius of the artery at point 0:

$$[Uu_z - u_z u_y]_0^{r_0} + \int_0^{r_0} (U - u_z)(u_y/y)\,\mathrm{d}y - \frac{\partial}{\partial z}\int_0^{r_0} (u_z^2 - Uu_z)\,\mathrm{d}y + \frac{\mathrm{d}U}{\mathrm{d}z}\int_0^{r_0} (U - u_z)\,\mathrm{d}y = -\frac{\mu}{\rho}\left[\frac{\partial u_z}{\partial y}\right]_0^{r_0}. \quad (4)$$

Similar equations are obtained at points 1 and 2, where the upper limits in the integrals will be r_1 and r_2. We can reduce the right-hand side of Eq. (4) by noting that $\partial u_z/\partial y = 0$ at $y = r_0$, and $\mu(\partial u_z/\partial y)$ at $y = 0$ is simply the negative of the wall shear stress, $-\tau_w$.

We now define quantities θ and δ^*:

$$\theta = \int_0^{r_0} \frac{u_z}{U}\left(1 - \frac{u_z}{U}\right)\mathrm{d}y, \quad (5)$$

$$\delta^* = \int_0^{r_0} \left(1 - \frac{u_z}{U}\right)\mathrm{d}y, \quad (6)$$

which are identical to the plane two-dimensional momentum and displacement thicknesses (White, 1991). In cylindrical coordinates we can retain the plane definitions or use the physically correct θ and δ^* (Schlichting, 1979). It is simpler and mathematically as effective to retain the two-dimensional definitions.

Introducing definitions (5) and (6) into Eq. (4) and setting $u_y = 0$ at $y = 0$ and $u_z = U_0$ at $y = r_0$:

$$U_0 \int_0^{r_0} \left(1 - \frac{u_z}{U_0}\right)\frac{u_y}{y}\,\mathrm{d}y + \frac{\partial}{\partial z}(U_0^2\theta_0) + U_0\frac{\mathrm{d}U_0}{\mathrm{d}z}\delta_0^* = \frac{\tau_w}{\rho}. \quad (7)$$

The first term on the left-hand side may be integrated by parts, and can be shown to be zero. Rearranging, generalising to any axial point along the artery by dropping subscripts, and introducing the shape factor $H = \delta^*/\theta$, we obtain the momentum integral relation

$$\frac{\mathrm{d}\theta}{\mathrm{d}z} + (2 + H)\frac{\theta}{U}\frac{\mathrm{d}U}{\mathrm{d}z} = \frac{\tau_w}{\rho U^2}. \quad (8)$$

This relation for cylindrical systems is the same as that for the two-dimensional planar case.

2.3. Thwaites' method for cylindrical flows

Thwaites (1949) developed a one-parameter correlation method for solving the integral momentum equation (8) to an accuracy, typically within 3% (White, 1991). The technique was originally developed for solving two-dimensional planar problems but, as shown above, the integral momentum equation for problems with cylindrical geometry is identical if the same symbolic definitions of θ and δ^* are used (Rott and Crabtree, 1952; Schlichting, 1979).

The momentum thickness, θ, given by Eq. (5) can be approximated at any point z measured from a stagnation point by

$$\theta^2 = \frac{0.45\mu}{\rho U^6}\int_0^z U^5\,\mathrm{d}z, \quad (9)$$

where the constant parameters in Eq. (9) were derived by Thwaites (1949) from known analytic and experimental boundary layer results. Using θ we obtain the parameter

$$\lambda = \frac{\rho\theta^2}{\mu}\frac{\mathrm{d}U}{\mathrm{d}z} \quad (10)$$

The shear and shape function correlations suggested by White (1991) are

$$S(\lambda) \approx (\lambda + 0.09)^{0.62}, \quad (11)$$

$$H(\lambda) \approx 2.0 + 4.14k - 83.5k^2 + 854k^3 - 3337k^4 + 4576k^5, \quad (12)$$

where $k = 0.25 - \lambda$. Finally, the wall shear stress and the displacement thickness are calculated via

$$\tau_w = \frac{\mu U}{\theta}S(\lambda), \quad (13)$$

$$\delta^* = \theta H(\lambda). \quad (14)$$

Eqs. (13), (11) and (10) indicate that the maximum wall shear stress occurs where the gradient of the axial velocity is finite. The velocity gradient is zero at the stenosis throat, so the maximum wall shear stress will occur just ahead of the throat, where the flow is still accelerating. This observation is in agreement with the reported CFD results (Huang et al., 1995; Sarin and Mehrotra, 1992).

2.4. The numerical procedure

Employing Thwaites' equation (9), the momentum thickness at the throat is

$$\theta_2^2 = \frac{0.45\mu}{\rho U_2^6}\int_{z=0}^{z=z_2} U^5\,\mathrm{d}z, \quad (15)$$

where $z = 0$, is a stagnation point and the subscripts correspond to points in Fig. 1. This integral can be split

into two

$$\theta_2^2 = \frac{0.45\mu}{\rho U_2^6}\left(\int_{z=0}^{z=z_1} U^5\,\mathrm{d}z + \int_{z=z_1}^{z=z_2} U^5\,\mathrm{d}z\right). \tag{16}$$

The first term in the bracket of Eq. (16) is, from Eq. (9),

$$\int_{z=0}^{z=z_1} U^5\,\mathrm{d}z = \frac{\rho\theta_1^2 U_1^6}{0.45\mu}, \tag{17}$$

so Eq. (16) becomes

$$\theta_2^2 = \theta_1^2\left(\frac{U_1}{U_2}\right)^6 + \frac{0.45\mu}{\rho U_2^6}\int_{z=z_1}^{z=z_2} U^5\,\mathrm{d}z. \tag{18}$$

The momentum thickness in the upstream parabolic Poiseuille flow is $\theta_1 = 2r_1/15$, from Eq. (5).

The integration in Eq. (18) can be performed numerically provided the velocity distribution through the stenosis and at the throat are known. The simplest assumption is that the peak velocity varies linearly through the stenosis. This also makes the derivative in Eq. (10) straightforward to calculate.

The centreline velocity at point 1, U_1, is the maximum velocity in Poiseuille flow, i.e. twice the mean velocity. The published results normally quote the upstream Reynolds number, which is related to the volumetric flow rate, Q in $\mathrm{m^3\,s^{-1}}$, via

$$Re = \frac{2\rho Q}{\pi r_1 \mu}, \tag{19}$$

while

$$U_1 = \frac{Re\mu}{r_1\rho}. \tag{20}$$

A first estimate for the centreline velocity in the stenosis throat is the mean velocity there, assuming the inviscid core velocity profile extends across the entire throat. From conservation of volume,

$$U_2 = \frac{U_1 r_1^2}{2r_2^2}. \tag{21}$$

This estimate can be substantially improved by using the displacement thickness. At the throat, $H(\lambda) = 2.61$ by Eqs. (10) and (12), and the displacement thickness will be $\delta_2^* = 2.61\theta_2$ by Eq. (14). So the flat velocity profile is a reasonable approximation over the radius $r_2' = r_2 - \delta_2^*$, which should be used in Eq. (21) instead of r_2.

An iterative scheme can be developed:

(1) Set the effective throat radius, r_2, to the actual throat radius.
(2) Calculate the momentum thickness θ_2 from Eq. (18), using Eq. (21).
(3) Calculate the displacement thickness, $\delta_2^* = 2.61\theta_2$.
(4) Calculate the new effective throat radius $r_2 = r_2 - \delta_2^*$.
(5) Repeat from step 2 until there is no change in effective radius.

In practice, it is necessary to introduce some 'underrelaxation' in step 4 so that the full radius correction, δ_2^*, is not implemented at each step, as for low flow rates or moderate stenoses early iterates for δ_2^* can be greater than the actual throat radius.

Using the converged results for θ_2 and assuming linear variation of peak velocity through the stenosis, Eqs. (10), (11) and (13) yield the wall shear stress just ahead of the stenosis throat. The geometrical parameters which affect this shear stress are the axial length and radial height of the stenosis.

3. Results

We have implemented the model on a PC under BASIC and MATLAB. The program runs to some 100 lines of BASIC or 40 lines of MATLAB code and takes fewer than 15 s to calculate shear stresses for any given set of stenosis geometry and flow parameters. The inputs needed are R and L (the radial height and axial length of the stenosis in units of r_1), and the physiological parameters r_1, ρ, μ, and Re. Results from the model will now be compared to published data.

Huang et al. (1995) and Back and Crawford (1992) report numerical results for shear stress in stenosed geometries. The five stenoses modelled by Huang et al. are smooth and conical. Their geometrical characteristics are listed in Table 1 (models M1–M5). Back and Crawford also assume a conical geometry and their single model is denoted M6 in Table 1. The area reduction due to the stenosis is $R(2 - R)$.

Numerical simulations of models M1–M5 are reported using the physiological parameters $r_1 = 3.5 \times 10^{-3}$ m, $\rho = 1060\ \mathrm{kg\,m^{-3}}$, $\mu = 3.71 \times 10^{-3}\ \mathrm{N\,s\,m^{-2}}$, for $Re =$ 100, 500, 1000. Results from model M6 are reported using $r_1 = 1.54 \times 10^{-3}$ m, $\rho = 1050\ \mathrm{kg\,m^{-3}}$, $\mu = 3.68 \times 10^{-3}$ $\mathrm{N\,s\,m^{-2}}$, for $Re = 59$, 83, 207, 353. Our predictions of shear stress can be compared to these results and also shear stress calculations assuming Poiseuille flow. If the flow remained Poiseuille-like throughout the stenosis, the wall shear stress at the throat would be (White, 1991)

$$\tau_{w,p} = 2\mu U_1 \frac{r_1^2}{r_2^3}. \tag{22}$$

Table 1
Model stenosis geometric parameters. The radial height, R, and axial length, L, of the stenosis are given in units of the arterial radius, r_1, for published stenosis models M1–M5 (Huang et al., 1995) and M6 (Back and Crawford, 1992)

	M1	M2	M3	M4	M5	M6
R	1/4	1/3	1/2	1/2	1/2	3/10
L	4	4	4	8	2	14
Area reduction (%)	44	56	75	75	75	51

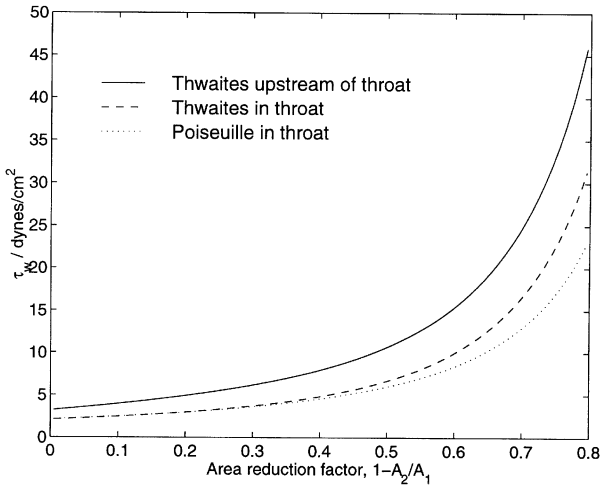

Fig. 3. Variation of shear stress with area reduction in stenosis, for $Re = 100$, $L = 4$. Comparison of results from the present model with Poiseuille flow.

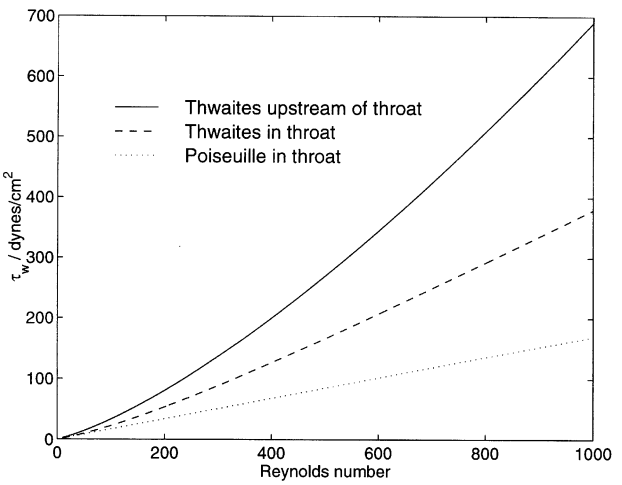

Fig. 4. Variation of shear stress with Reynolds number for stenosis M3 (75% contraction). Comparison of results from the present model with Poiseuille flow.

Fig. 3 demonstrates that for stenoses over the range of 0–80% area reduction our model predicts higher shear stresses, compared to Poiseuille predictions, both in the throat and just upstream of the throat. The results labelled 'Thwaites in throat' have been obtained by setting the velocity gradient, and therefore λ, to zero. The results in Fig. 3, for $Re = 100$ and $L = 4$, show that for decreasingly prominent stenoses the Thwaites and Poiseuille calculations at the throat converge. This behaviour is expected, as disruption of Poiseuille-like flow in the stenosis decreases with decreasing occlusion (Sarin and Mehrotra, 1992). The convergence of the two results indicates the general validity of the present method and its applicability across the entire range of stenosis severity. Conversely, the present method correctly predicts the higher observed values of shear stress which Poiseuille assumptions fail to capture.

Fig. 4 shows the variation in shear stress at, and upstream of, the throat over the range of physiologically common Reynolds numbers ($Re = 10$–1000) for the stenosis model M3. At high Reynolds numbers the difference between results calculated using the present method and assuming Poiseuille flow is substantial. At low Reynolds numbers, the model results converge to the Poiseuille results. This is expected because in a slow flow the boundary layers have time to adjust to the constriction of the stenosis, thereby maintaining Poiseuille-like behaviour. That our model identifies this feature indicates its applicability across the physiological range of arterial Reynolds numbers.

Comparisons with the reported CFD simulations are shown in Figs. 5 and 6, and Table 2. The shear stress results from our model are those calculated just upstream of the stenosis throat. Over the range of flow conditions and stenosis geometries examined, the rms average error

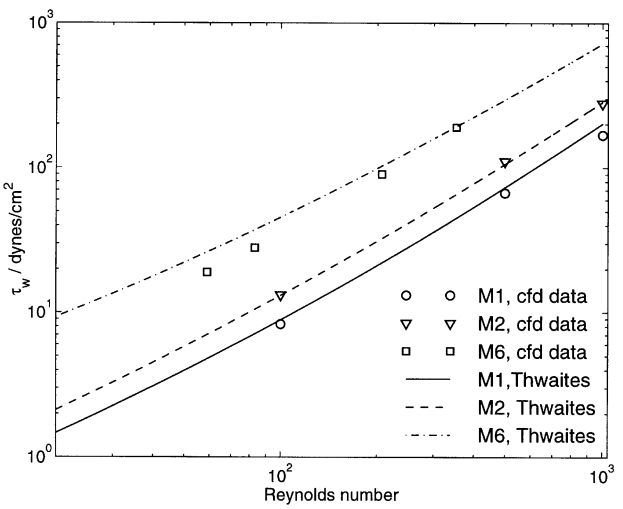

Fig. 5. Comparison of reported CFD data (symbols) of shear stress with predictions of the present model (lines), for mild and moderate stenoses M1, M2, M6.

between our model results and reported CFD simulations is 13%. Fig. 5 shows this good agreement between reported simulations and the present model over the range of Reynolds numbers from 20 to 1000 for moderate stenoses ($< 75\%$ occlusion, models M1, M2 and M6). The agreement is excellent, as Back and Crawford (1992) report the accuracy for their data for model M6 to be about 15%. The accuracy of the data provided by Huang et al. (1995) for models M1–M5 is unknown. A good correlation with CFD data for severe stenoses ($\geqslant 75\%$ occlusion, models M3–M5) is also displayed in Fig. 6. The present method only slightly underestimates shear stress values, but clearly follows the data trend. These three stenoses have the same contraction, but our results

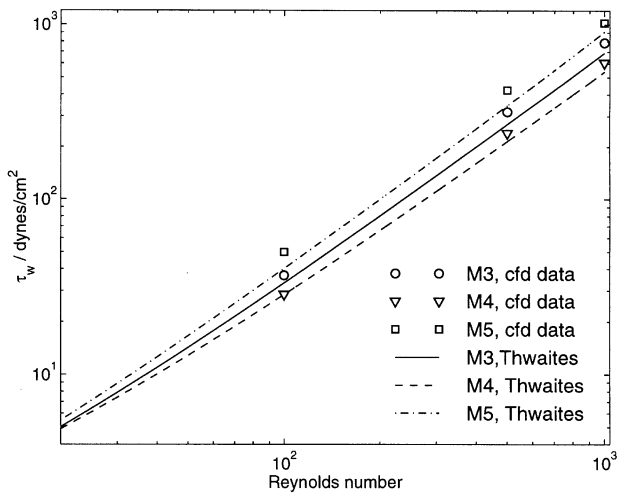

Fig. 6. Comparison of reported CFD data (symbols) of shear stress with predictions of the present model (lines), for severe stenoses M3, M4, M5, all 75% contraction with varying lengths.

Table 2
Calculated peak (upstream of throat) shear stress in dyn cm^{-2} for stenosis models M1–6 at Reynolds numbers in the range $Re = 59$–1000. Figures in paranthesis are previously published results of calculations by Back and Crawford (1992) and Huang et al. (1995)

Re	M1	M2	M3	M4	M5	M6
59	—	—	—	—	—	26.2 (19.0)
83	—	—	—	—	—	37.4 (28.0)
100	8.9 (8.3)	13.1 (13.2)	33.2 (36.7)	28.5 (28.6)	40.2 (49.9)	—
207	—	—	—	—	—	102.7 (90.0)
353	—	—	—	—	—	192.9 (190.0)
500	73.3 (67.1)	105.8 (110.6)	269.6 (316.9)	215.2 (240.3)	345.1 (423.2)	—
1000	201.7 (168.3)	285.2 (279.2)	690.2 (788.1)	539.1 (607.7)	910.2 (1022.7)	—

confirm the systematic increase of shear stress with decreasing length.

4. Discussion

Our predictions of wall shear stress agree closely with the limited available data. As a tool for biomedical researchers, our model is simple to implement and provides useful information on the dependency of shear stress on stenosis geometry and flow conditions. Back and Crawford (1992) noted that a real stenosis is not smooth, and diffuse atherosclerotic disease causes local wall irregularities, but a mean, conical approximation does not substantially affect the results. At very high Reynolds numbers, or for more severe or axially non-symmetric stenoses, there may be flow separation downstream of the throat — the boundary layer will lift off the surface of the artery. But as this leads to lower wall shear stresses in the stagnant region, it is not considered here. Also the maximum wall shear stress does not depend on any axial asymmetry of the stenosis (Srivastava, 1995).

The validity of Thwaites' method for the laminar boundary layer calculations can be assessed by comparison to Poiseuille flow in a pipe, to provide a maximum bound on the expected error. In incompressible constant-radius pipe flow, the velocity does not vary in the axial direction but the total pressure falls slowly, unlike boundary layer flows where acceleration and pressure gradient are linked. Through the stenosis, however, the flow accelerates and the negative pressure gradient is higher. For fully developed flow, with a *peak* velocity U, in a pipe of radius r, the pressure gradient is (White, 1991)

$$\frac{\mathrm{d}p}{\mathrm{d}z} = -\frac{2\mu U}{r^2} = -\frac{\tau_w}{r}. \tag{23}$$

The actual displacement and momentum thicknesses may be evaluated using the true definitions of δ^* and θ (White, 1991). Given the classic parabolic velocity distribution, this would yield $\delta^* = r/4$, and $\theta = r/12$. The shape factor would then be $H = (r/4)/(r/12) = 3$, quite beyond the range of validity of Thwaites' method.

Our interpretation of Thwaites' method is that the total pressure is presumed constant and the centreline velocity may be regarded as the velocity at the edge of a boundary layer on each wall. Eqs. (3) and (10) yield

$$\frac{\mathrm{d}p}{\mathrm{d}z} = -\frac{\mu U \lambda}{\theta^2}. \tag{24}$$

Comparing Eqs. (23) and (24) suggest an 'equivalent λ' for Poiseuille flow; $\lambda = 4\theta^2/r^2$. Thwaites' method, even in its axisymmetric formulation, for a constant-radius pipe, uses Eqs. (5) and (6). So $\theta = 2r/15$ for a parabolic Poiseuille flow and $\lambda = 16/225$. Substituting *this* value for the correlation parameter into Eqs. (11) and (13) yields $S = 0.322$ and $\tau_w = 2.42\mu U/r$. This shows that the match between the exact and approximate results, for a worst-case fully developed internal flow, is within 21%. The shape factor, $H = 2.38$ from Eq. (13), is characteristic of a mildly accelerating flow. This is sufficiently good to justify proceeding with the classical Thwaites' method. In the stenosis, predictions are expected to be more accurate because the flow strongly accelerates.

5. Conclusion

A simple model has been derived from laminar boundary layer theory to investigate the flow of blood in arterial

stenoses up to Reynolds numbers of 1000. Apart from physiological flow data, the only information required is the height and length of the stenosis. The model accurately predicts the wall shear stress for all physical flow rates and stenosis severities, without the need for intensive computational fluid dynamics simulations. Agreement with published CFD results is within 13% rms.

The model can be implemented on a good programmable calculator or PC and should be a useful tool for biomedical investigations. The agreement between our model and reported numerical results allows the examination of a wide flow and geometrical parameter region. Future development should include further validation of the model against CFD and experimental data, the incorporation of pulsatile non-Newtonian blood flow, nonconical stenoses and the elastic motion of the arterial wall.

References

Back, L.H., Crawford, D.W., 1992. Wall shear stress estimates in coronary constrictions. Journal of Biomechanical Engineering 114, 515–520.

Damodaran, V., Rankin, G.W., Zhang, C., 1996. Numerical study of steady laminar flow through tubes with multiple constrictions using curvilinear co-ordinates. International Journal of Num. Meth. Fluids 23, 1021–1041.

Houston, P., Dickson, M.C., Ludbrook, V., White, B., Schwachtgen, J.-L., McVey J.H., Mackman, N., Reese, J.M., Gorman, D.G., Campbell, C., Braddock, M., 1999. Fluid shear stress induction of the tissue factor promoter *in vitro* and *in vivo* is mediated by Egr-1. Arteriosclerosis, Thrombosis and Vascular Biology (accepted).

Huang, H., Mofi, V.J., Seymour, B.R., 1995. Fluid mechanics of stenosed arteries. International Journal of Engineering Science 33(6), 815–828.

Johnston, P.R., Kilpatrick, D., 1991. Mathematical modelling of flow through an irregular arterial stenosis. Journal of Biomechanics 24(11), 1069–1077.

Ku, D.N., 1997. Blood flow in arteries. Annual Review of Fluid Mechanics 29, 399–434.

Morgan, B.E., Young, D.F., 1974. An integral method for the analysis of flow in arterial stenoses. Bulletin of Mathematical Biology 36, 39–53.

Rosenson, R.S., McCormick, A., Uretz, E.F., 1996. Distribution of blood viscosity values and biochemical correlates in healthy adults. Clinical Chemistry 42(8), 1189–1195.

Rott, N., Crabtree, L.F., 1952. Simplified laminar boundary-layer calculations for bodies of revolution and for yawed wings. Journal of Aeronautical Science 19, 553–565

Sarin, V.B., Mehrotra, R., 1992. Stenotic effects in a tube of elliptic cross-section at low Reynolds numbers. International Journal of Biomedical Computing 30, 137–146.

Schlichting, H., 1979. Boundary-Layer Theory. McGraw-Hill, New York.

Skalak, R., Özkaya, N., Skalak, T.C., 1989. Biofluid mechanics. Annual Review of Fluid Mechanics 21, 167–204.

Srivastava, V.P., 1995. Arterial blood flow through an nonsymmetrical stenosis with applications. Japanese Journal of Applied Physics 34, 6539–6545.

Thwaites, B., 1949. Approximate calculation of the laminar boundary layer. Aeronautical Quarterly 1, 245–280.

White, F.M., 1991. Viscous Fluid Flow, McGraw-Hill, Singapore.